Ionics (2016) 22:1387–1393
DOI 10.1007/s11581-016-1661-x

ORIGINAL PAPER

Synthesis and electrochemical investigation of highly dispersed ZnO nanoparticles as anode material for lithium-ion batteries

Haipeng Li[1,2,3] · **Yaqiong Wei**[1,2,3] · **Yongguang Zhang**[1,2] · **Fuxing Yin**[1,2] · **Chengwei Zhang**[1,2] · **Gongkai Wang**[1,2] · **Zhumabay Bakenov**[4]

Received: 24 October 2015 / Revised: 17 January 2016 / Accepted: 27 January 2016 / Published online: 10 February 2016

Abstract Highly dispersed ZnO nanoparticles were prepared by a versatile and scalable sol-gel synthetic technique. High-resolution transmission electronic microscopy (HRTEM) showed that the as-prepared ZnO nanoparticles are spherical in shape and exhibit a uniform particle size distribution with the average size of about 7 nm. Electrochemical properties of the resulting ZnO were evaluated by galvanostatic discharge/charge cycling as anode for lithium-ion battery. A reversible capacity of 1652 mAh g^{-1} was delivered at the initial cycle and a capacity of 318 mAh g^{-1} was remained after 100 cycles. Furthermore, the system could deliver a reversible capacity of 229 mAh g^{-1} even at a high current density of 1.5 C. This outstanding electrochemical performance could be attributed to the nano-sized features of highly dispersed ZnO particles allowing for the better accommodation of large strains caused by particle expansion/shrinkage along with providing shorter diffusion paths for Li^+ ions upon insertion/deinsertion.

Keywords Lithium ion battery · Anode · Highly dispersed ZnO nanoparticles · Sol-gel

✉ Yongguang Zhang
yongguangzhang@hebut.edu.cn

[1] Research Institute for Energy Equipment Materials, Hebei University of Technology, Tianjin 300130, China

[2] Tianjin key laboratory of laminating fabrication and interface control technology for advanced materials, Hebei University of Technology, Tianjin 300130, China

[3] School of Material Science and Engineering, Hebei University of Technology, Tianjin 300130, China

[4] Institute of Batteries LLC, PI Nazarbayev University Research and Innovation System, Nazarbayev University, 53 Kabanbay Batyr Avenue, Astana, Kazakhstan 010000

Introduction

Due to their superior energy density, stability, and long cycle life, lithium-ion batteries (LIBs) have been under intense scrutiny in the portable electronics industry [1, 2]. Since the first commercial LIBs were introduced by Sony Corporation in 1991, graphite was one of the most widely used anode materials for these batteries [3]. However, its low theoretical capacity (372 mAh g^{-1}) limits its application especially in rapidly developing large-scale energy storage and electricity powered transport, which demands high-energy density batteries. Therefore, the development of alternative high-performance anodes for LIBs is crucially required.

In order to overcome the mentioned problem, transition metal oxides (MO, M = Fe, Cu, Ni, Co, etc.) have been explored as potential anode materials. Functioning through a reversible electrochemical conversion between metal nanoparticles and metal oxides, transition metal oxides generally show a larger specific capacity than graphite [4]. Among various transition metal oxides, zinc oxide (ZnO) has been recognized as a more intriguing one due to its advantages, such as low cost, facile preparation, and chemical stability, and, more importantly, ZnO possesses a high theoretical capacity of 978 mAh g^{-1} based on the following electrochemical reaction of ZnO with Li-ions [5]:

$$ZnO + 2Li \rightleftarrows Zn + Li_2O \quad (1)$$

$$Zn + Li \rightleftarrows LiZn \quad (2)$$

The overall reaction:

$$ZnO + 3Li \rightleftarrows LiZn + Li_2O \quad (3)$$

However, large volume changes of ZnO particles during charge/discharge pose a serious challenge in its application as a LIBs anode material when ZnO is transformed into Zn upon a redox reaction (1) and the following alloying reaction of formation of Li-Zn (2), the accompanying volume changes could be up to ~228 %, which is much larger than that of graphite (~10 %) [6, 7], leading to the material rupture and consequent capacity fading. Therefore, a lot of efforts have been devoted to overcome this problem and improve the electrochemical performance of ZnO anode. It is well-recognized that nanostructured materials not only effectively accommodate the large strains resulted from the volume expansion/shrinkage but also provide short diffusion paths for Li-ions [8], which allows for remarkable enhancement of electrochemical performance. Therefore, an effective nanostructural design for ZnO is a promising approach to prepare a high-performance anode, and, therefore, requires systematic comparative studies. Recently, numerous ZnO-based nanostructures were designed and proposed, including ZnO nanosheets, ZnO nanofibers, and ZnO nanoflowers, and enhanced electrochemical performance of the material was reported [8–10].

Nevertheless, to the best of our knowledge, a versatile and scalable synthesis of dispersed ZnO nanoparticles as anode material for LIBs is rarely reported. Herein, we present the synthesis of novel highly dispersed ZnO nanoparticles via sol-gel method, and investigation of its physical and electrochemical properties as an anode for LIBs.

Experimental

Sol-gel technique was used to prepare dispersed ZnO nanoparticles. All reagents were purchased from Tianjin Fuchen Chemical Company and used without further purification. ZnO sols were prepared using zinc acetate ($Zn(CH_3COO)_2$, ≥99 %); ethanol (C_2H_5OH, ≥99.7 %); and lithium hydroxide (LiOH, ≥90 %). In a typical experiment, 2.860 g $Zn(CH_3COO)_2$ and 0.754 g LiOH was dissolved separately each in 130-mL ethanol. Both samples were stirred for 30 min, and the LiOH solution was slowly added into the $Zn(CH_3COO)_2$ solution. A white sol was formed, which was stirred for 24 h. The white precipitate was separated via filtration, thoroughly washed with deionized water and ethanol, and then vacuum dried overnight at 60 °C.

The crystalline phases of the sample were determined by x-ray diffraction (XRD, SmartLab, Rigaku Corporation) equipped with Cu Kα radiation. The thickness and morphology of the sample was investigated using an atomic force microscope (AFM, 5500 Agilent Technologies) in air. Its interior structure was examined using transmission electron microscopy (TEM, JEM-2100F, JEOL) at 160 kV. The electrochemical performance of the sample was investigated using coin-type cells (CR2025). Lithium foil was used as both the counter and the reference electrodes. Then, 1 mol dm^{-3} $LiPF_6$ dissolved in a mixture of dimethyl carbonate/diethyl carbonate/ethylene carbonate (1:1:1 by volume) was used as an electrolyte, and microporous polypropylene film was used as a separator. The ZnO electrode was prepared by mixing 70 wt% as-prepared ZnO nanoparticle powder, 10 wt% polyvinylidene fluoride (PVDF) (Kynar, HSV900) as a binder and 20 wt% acetylene black (MTI, 99.5 % purity) as a conducting agent in 1-methyl-2-pyrrolidinone (NMP, Sigma-Aldrich, ≥99.5 % purity). The resultant slurry was uniformly spread onto nickel foam using a doctor blade and dried at 50 °C for 12 h. The resulting ZnO film was used to prepare the electrodes by punching circular disks with 1 cm in diameter. The active material loading in each electrode was about 2 mg cm^{-2}. The coin-type cells were assembled in an Ar (99.9995 %) filled glove box (MBraun) and tested galvanostatically on a multichannel battery tester (BTS-5V5mA, Neware) in a cutoff potential window of 0.005–3.0 V vs. Li^+/Li electrode at different current densities. All electrochemical measurements were performed at room temperature. Cyclic voltammetry (CV) was carried out on an electrochemical workstation (CHI 660D, CH Instruments Inc.) at a scan rate of 0.1 mV s^{-1} in the potential range of 0–3.0 V vs. Li^+/Li. Electrochemical impedance spectroscopy (EIS) was measured by using the CHI 660D electrochemical workstation within a frequency range of 0.01–100 kHz.

Results and discussion

The XRD analysis was performed to investigate the crystal phase of the as-prepared sample. Figure 1 shows the characteristic XRD patterns of the as-prepared ZnO, which can be assigned to the zincite (a = 0.3249 nm, c = 0.5206 nm, JCPDS

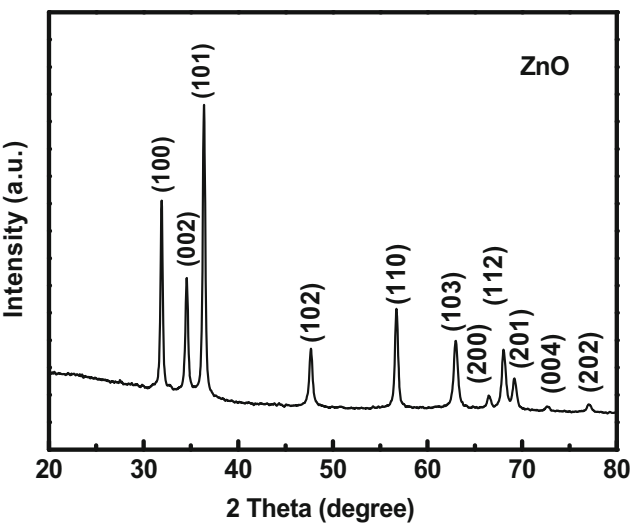

Fig. 1 XRD patterns of as-prepared ZnO sample

card No. 36–1451) [11]. Pronounced peaks located at 31.8°, 34.4°, 36.3°, 47.6°, 56.6°, 62.9°, 66.4°, 67.9°, 69.1°, 72.6°, and 76.9° could be indexed as (100), (002), (101), (102), (110), (103), (200), (112), (201), (004), and (202) planes of zincite [12], respectively. No impurities peaks were detected in the XRD patterns, which confirm the formation of pure ZnO. The average crystalline size of the highly dispersed ZnO nanoparticles was calculated based on the main (101) peak using the Debye-Scherrer formula. The average crystalline size was found to be around 6.7 nm.

The high-resolution transmission electronic microscopy (HRTEM) images of ZnO nanoparticles are presented in Fig. 2a and show that highly dispersed discrete and nearly spherical nanoparticles of ZnO were successfully synthesized by the present technique. The HRTEM data were used to determine the average mean diameters of the prepared particles. Figure 2b shows that the as-prepared ZnO nanoparticles have narrow particle size distribution with a geometric mean diameter of $d_{g,p}$ = 6.61 nm and a geometric standard deviation of σ_g = 1.20. These dimensions are consistent with the data obtained above using the Debye-Scherrer formula. As it can be seen at a higher magnification in Fig. 2c, the material exhibits a fringe lattice spacing of about 0.148 nm, which corresponds to the *d* spacing of (103) plane of ZnO [13]. This observation agrees with the XRD results as well. The crystallization of ZnO nanoparticles was further confirmed by HRTEM equipped with selected area electronic diffraction (SAED). As shown in Fig. 2d, all the diffraction rings in the SAED patterns of nanoparticles can be indexed as the ZnO phase (JCPDS card no. 36–1451) [14].

The sample was further characterized using AFM. The AFM analysis results (Fig. 3) show that the sample surface contains the ZnO clusters. These clusters have the diameters of about 80 nm and a height of ≤8.5 nm. It is quite interesting that the height of the cluster matches well with the average size of the ZnO particles obtained from the TEM data. This observation indicates that aggregation of the ZnO nanoparticle occurs with formation of only monolayered clusters. This seems to conflict with the TEM results, in which highly dispersed ZnO particles with average size of 6.6 nm were observed. In fact, the sample was sonicated before the TEM analysis, and this operation could cause destruction of the agglomerates; this implies that the aggregation of the ZnO nanoparticles could be mainly due to the physical attractive interaction, and therefore can be very easily separated during sonication treatment. Accordingly, aggregation of the electrode material particles does not limit its potential application as promising anode for LIBs, as it was confirmed in the following electrochemical studies.

The electrochemical properties of the nanostructured ZnO anode were investigated by CV. Figure 4 presents the initial CV curves of the electrode. In the cathodic part of the first

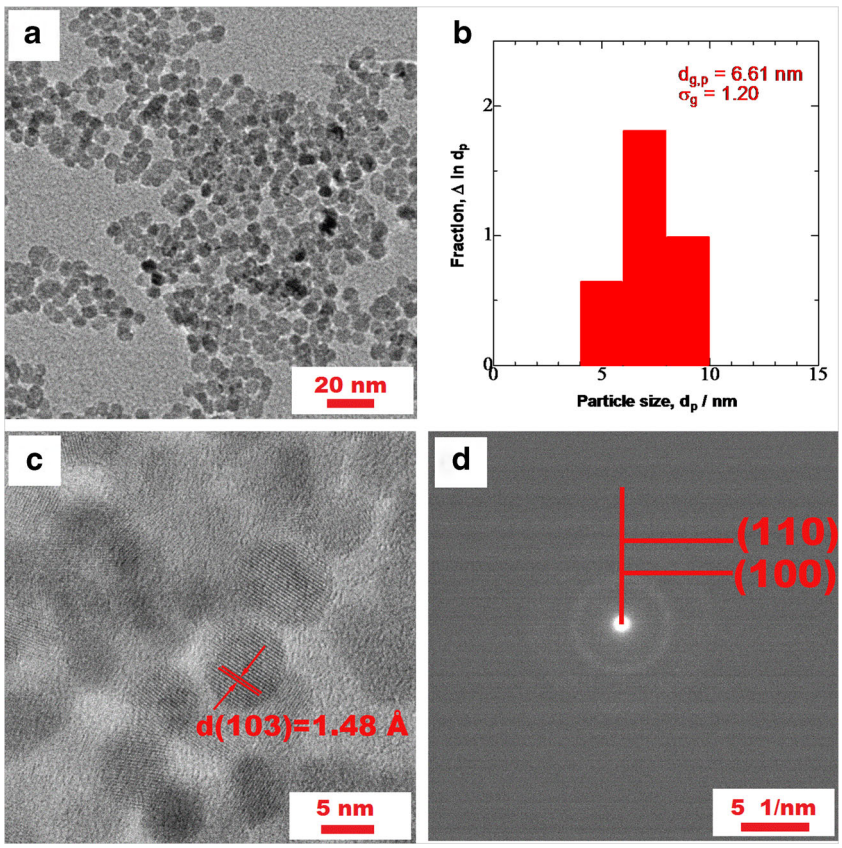

Fig. 2 **a** HRTEM images of as-prepared ZnO sample. **b** ZnO nanoparticles particle size distribution. **c** HRTEM image of ZnO sample. **d** SAED patterns of ZnO sample

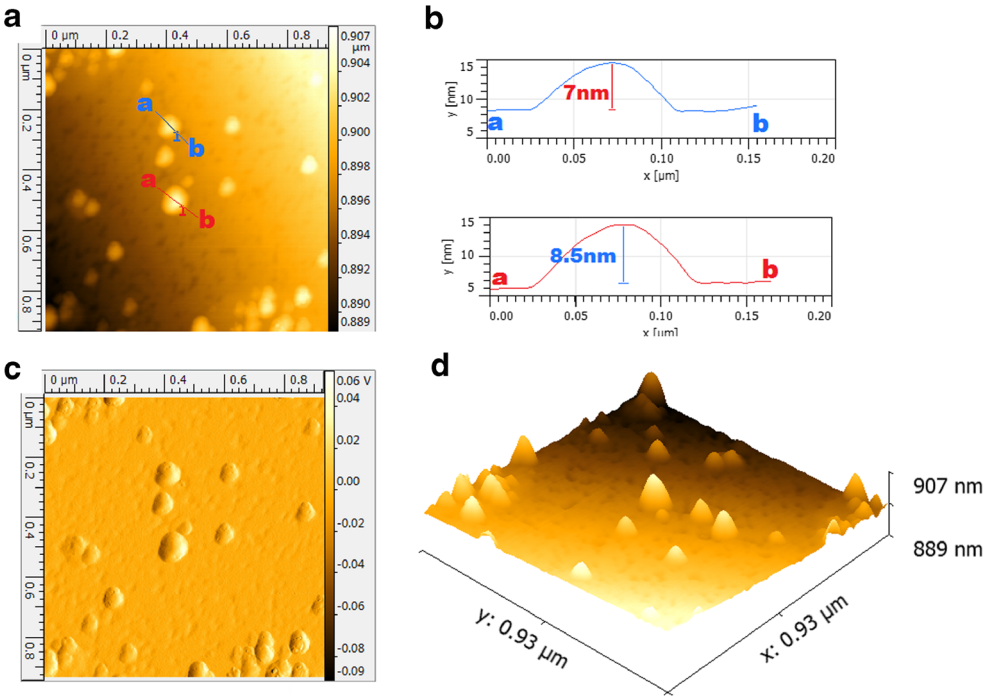

Fig. 3 **a** Two profiles extracts from two different regions in the micrographs with corresponding amplitude images of (**b**). **c** Two-dimensional AFM images of ZnO nanoparticle. **d** Three-dimensional AFM images of ZnO nanoparticle

cycle, the cell exhibits a prolonged tail and a low current peak, which correspond to the formation of the solid electrolyte interphase (SEI) layer [15–19]. The anodic scan of this cycle is characterized by a peak around 1.5 V vs. Zn^{+}/Zn, which is attributed to a multi-step dealloying process of Li-Zn alloy [8, 20]. It can be seen that the cathodic sweeps for the following cycles differ from the first one and have a well-defined peak at around 0.5–0.6 V corresponded to the processes described by Eqs. (1) and (2). In the same time, the anodic peaks of the second and third cycle are similar to that of the first cycle, which indicates a highly reversible character of the insertion/extraction reactions of the prepared ZnO electrode [20].

The initial profiles of the galvanostatic charge/discharge tests of the ZnO electrode are shown in Fig. 5. At the first cycle, there exists a prolonged potential slope at 0.5–0.6 V, which reflects the initial irreversible capacity loss, related to the SEI layer formation [21], which was also observed from the CV results earlier. It can be seen that the SEI formation process is inherent to the first cycle only and disappears in the following cycles, which exhibit relatively steady discharge and charge (lithiation/delithiation) processes with a high coulombic efficiency.

Figure 6 presents the cycling performance of the ZnO electrode at 0.1 C (1 C = 978 mA g^{-1}). The highly dispersed ZnO nanoparticles deliver a high initial discharge capacity of about 1652 mAh g^{-1} and maintain a reversible capacity of 318 mAh g^{-1} over 100 cycles with a capacity loss of only 0.3 % per cycle after the

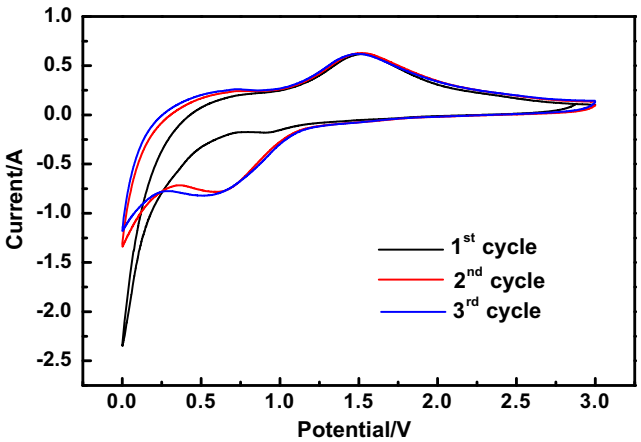

Fig. 4 Cyclic voltammograms of ZnO anode between 0.01 and 3.0 V vs. Li^{+}/Li at a scan rate of 0.1 mV s^{-1} at room temperature

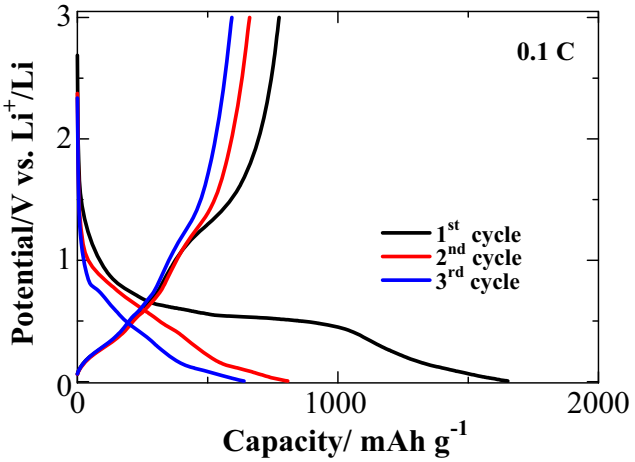

Fig. 5 Discharge/charge profiles of a lithium cell with ZnO electrode at 0.1 C

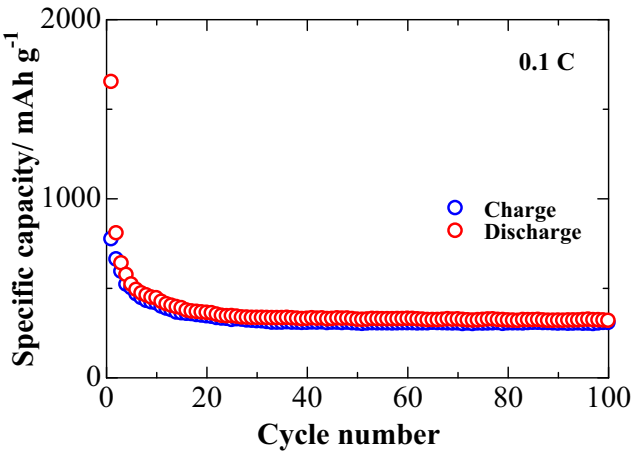

Fig. 6 Cycle performance of lithium cells with ZnO electrode at 0.1 C

first 10 cycles. In addition, this prolonged cycling is accompanied with a high coulombic efficiency (above 90 %). This performance enhancement could be attributed to the effective accommodation of the mechanical strain by the highly dispersed ZnO nanoparticles [8]. It should be noted that the phenomenon of enhanced volume change accommodation by reduced particle size has been reported for other electrode materials for LIBs and attributed to more flexible volume change capability of such systems [22–27].

The rate capability data of the ZnO electrode are presented in Fig. 7. It can be seen, that at a lower current density of 0.5 C, the electrode delivers a reversible discharge capacity of 550 mAh g^{-1} at the second cycle. There is a gradual capacity reduction with an increase in the cycling rate. At the higher current rate of 1 and 1.5 C, the reversible capacities of 313 and 229 mAh g^{-1} were sustained, respectively. It is worth noting, that the electrode recovers the most of its initial reversible capacity (329 mAh g^{-1}) when the discharge rate was modulated back to 0.5 C, indicating the high abuse tolerance of the electrodes containing highly

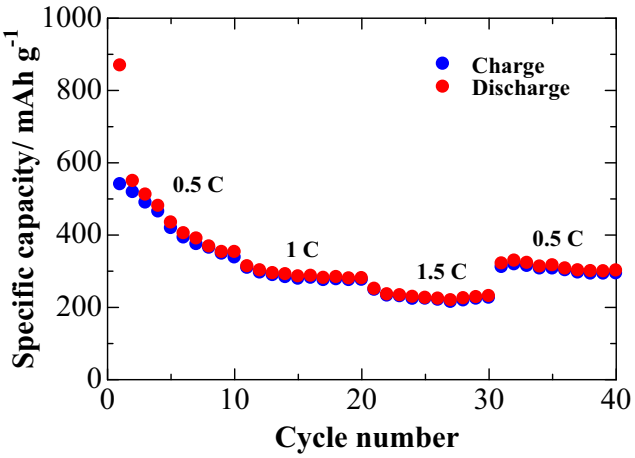

Fig. 7 Rate capability of lithium cells with the ZnO electrode

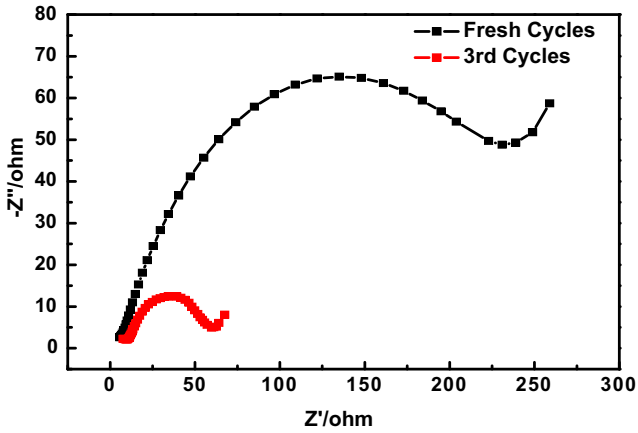

Fig. 8 EIS impedance spectra of fresh and cycled ZnO electrode

dispersed ZnO nanoparticles. This good rate performance is believed to be due to the highly dispersed nanoparticle structure, which along with accommodation of the volume changes upon cycling, provides short diffusion paths for lithium-ions, and large effective interfaces between the electrode particles and the electrolyte.

The EIS technique was used to analyze the impedance development trends of the ZnO anode upon its operation. Figure 8 presents typical Nyquist plots of a lithium cell with a fresh ZnO anode and after its three discharge/charge cycles: both plots consist of typical suppressed semicircles attributed to the charge transfer impedance, followed by a Warburg diffusion component [28, 29]. It can be seen that the cell impedance reduces upon cycling. This phenomenon could be due to formation of SEI on the electrode material surface providing enhanced charge transfer between its particles. This leads to an enhanced and stable electrochemical performance of the ZnO anode prepared in this work.

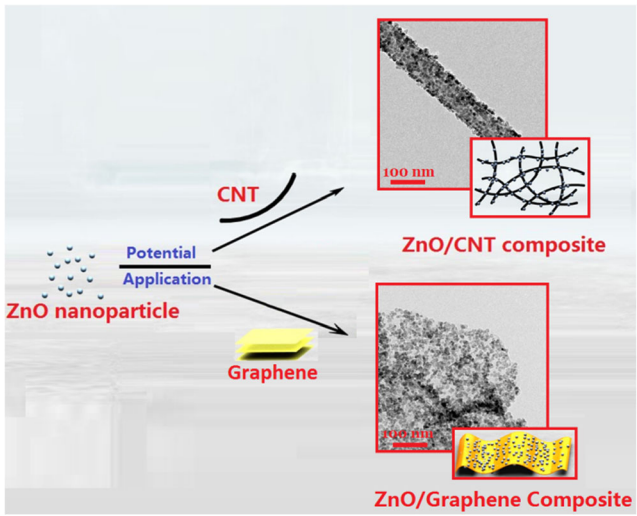

Fig. 9 Schematics of potential application of ZnO nanoparticles for high-performance electrodes preparation and further direction of the studies

The results of the studies on the ZnO nanoparticles synthesized in the present work provide insights on understanding of optimized design of this material as anode for LIBs. For example, introduction of highly dispersed ZnO nanoparticles into a second-phase host matrix, such as carbon nanotubes, graphene, and other carbonaceous frameworks, could enable preparation of a high-performance anode for LIBs. This could expand the materials practical applicability as anode for LIBs as it is schematically illustrated in Fig. 9 and planned in our future work on this material. Introduction of various host matrices with enhanced conductivity, specific surface area, and other features providing flexible conductive structures with enhanced accommodation of volume changes can further improve the electrochemical performance of the highly dispersed ZnO nanoparticles. Therefore, the present work could be considered as an example of a new approach to prepare the high performance ZnO based composites anodes for lithium-ion batteries. Further systematic studies are planned on the ZnO nanoparticle based composite anodes such as ZnO/CNT and ZnO/graphene composites and related systematically.

Conclusions

Highly dispersed ZnO nanoparticles with the average particle size of about 6.6 nm were successfully synthesized by a versatile and scalable sol-gel method. The composite electrode prepared using this material exhibited a very attractive electrochemical performance as an anode for lithium-ion batteries with the initial discharge capacity of 1652 mAh g^{-1} and a capacity of 318 mAh g^{-1} retained over 100 cycles. Moreover, the electrode exhibited a good rate capability, delivering a capacity of 229 mAh g^{-1} even at 1.5 C. These performance enhancements were attributed to an excellent dispersion of nano-sized ZnO: these features favor enhanced accommodation of the structure strains caused by the volume changes upon cycling, and provide short diffusion paths for Li^+ ions transport. The present work provides insights and new approaches for an optimized design of a high-performance ZnO composite anode for lithium-ion batteries, such as introduction of the highly dispersed ZnO nanoparticles into carbonaceous host frameworks to further improve their battery performance.

Acknowledgments The authors acknowledge the financial support from the National Natural Science Foundation of China (Grant No. 21406052), the Program for the Outstanding Young Talents of Hebei Province (grant no. BJ2014010), Natural Science Foundation of Hebei Province of China (project no. E2015202037), and Science and Technology Correspondent Project of Tianjin (project no. 14JCTPJC00496). ZB acknowledges the financial support by the grants from the Ministry of Education and Science of Kazakhstan #4649/GF.

References

1. Zhao Y, Zhang Y, Bakenov Z, Chen P (2013) Electrochemical performance of lithium gel polymer battery with nanostructured sulfur/carbon composite cathode. Solid State Ionics 23:40–45
2. Zhang Y, Zhao Y, Sun KE, Chen P (2011) Development in lithium/sulfur secondary batteries. Open Mater Sci J 5:215–221
3. Birrozzi A, Raccichini R, Nobili F, Marinaro M, Tossici R, Marassi R (2014) High-stability graphene nano sheets/SnO2 composite anode for lithium ion batteries. Electrochim Acta 137:228–234
4. Xiao L, Mei DD, Cao ML, Qu DY, Deng BH (2015) Effects of structural patterns and degree of crystallinity on the performance of nanostructured ZnO as anode material for lithium-ion batteries. J Alloys Compd 627:455–462
5. Yuan GH, Wang G, Wang H, Bai JT (2015) Synthesis and electrochemical investigation of radial ZnO microparticles as anode materials for lithium-ion batteries. Ionics 21(2):365–371
6. Lin YM, Abel PR, Heller A, Mullins CB (2011) α-Fe2O3 nanorods as anode material for lithium ion batteries. J Phys Chem Lett 2(22): 2885–2891
7. Ren ZM, Wang ZY, Chen C, Wang J, Fu XX, Fan CY, Qian GD (2014) Preparation of carbon-encapsulated ZnO tetrahedron as an anode material for ultralong cycle life performance lithium-ion batteries. Electrochim Acta 146:52–59
8. Huang XH, Xia XH, Yuan YF, Zhou F (2011) Porous ZnO nanosheets grown on copper substrates as anodes for lithium ion batteries. Electrochim Acta 56:4960–4965
9. Zhu J, Zhang GH, Gu SZ, Lu BG (2014) SnO_2 nanorods on ZnO nanofibers: a new class of hierarchical nanostructures enabled by electrospinning as anode material for high-performance lithium-ion batteries. Electrochim Acta 150:308–313
10. Chen XF, Huang Y, Zhang X, Li C, Chen JJ, Wang K (2015) Graphene supported ZnO/CuO flowers composites as anode materials for lithium ion batteries. Mater Lett 152:181–184
11. Gurav KV, Deshmukh PR, Lokhande CD (2011) LPG sensing properties of Pd-sensitized vertically aligned ZnO nanorods. Sensors Actuators B Chem 151(2):365–369
12. Jiang LQ, Gao L (2005) Fabrication and characterization of ZnO-coated multi-walled carbon nanotubes with enhanced photocatalytic activity. Mater Chem Phys 91(2–3):313–316
13. Huang XH, Wu JB, Lin Y, Guo RQ (2012) ZnO microrod arrays grown on copper substrates as anode materials for lithium ion batteries. Int J Electrochem Sci 7:6611–6621
14. Guo M, Diao P, Cai SM (2005) Hydrothermal growth of perpendicularly oriented ZnO nanorod array film and its photoelectrochemical properties. Appl Surf Sci 249(1–4):71–75
15. Yan JF, Wang G, Wang H, Zhang ZY, Ruan XF, Zhao W, Yun JN, Xu MZ (2015) Preparation and electrochemical performance of bramble-like ZnO array as anode materials for lithium-ion batteries. J Nanopart Res 17:52
16. Tian QH, Tian Y, Zhang ZX, Yang L, Hirano S (2015) Fabrication of CNT@void@SnO_2@C with tube-in-tube nanostructure as high-performance anode for lithium-ion batteries. J. Power Sources 291: 173–180
17. Lalia BS, Khalil A, Shah T, Hashaikeh R (2015) Flexible carbon nanostructures with electrospun nickel oxide as a lithium-ion battery anode. Ionics 21:2755–2762
18. Varghese B, Reddy M, Yanwu Z, Lit CS, Hoong TC, Subba Rao G, Chowdari B, Wee ATS, Lim CT, Sow CH (2008) Fabrication of NiO nanowall electrodes for high performance lithium ion battery. Chem Mater 20(10):3360–3336
19. Wen ZH, Wang Q, Zhang Q, Li JH (2007) In situ growth of mesoporous SnO_2 on multiwalled carbon nanotubes: A novel composite with porous-tube structure as anode for lithium batteries. Adv Funct Mater 17:2772–2778

20. Wang HB, Pan QM, Cheng YX, Zhao JW, Yin GP (2009) Evaluation of ZnO nanorod arrays with dandelion-like morphology as negative electrodes for lithium-ion batteries. Electrochim Acta 54:2851–2855
21. Hu C, Guo S, Lu G, Fu Y, Liu J, Wei H, Yan X, Wang Y, Guo Z (2014) Carbon coating and Zn^{2+} doping of magnetite nanorods for enhanced electrochemical energy storage. Electrochim Acta 148: 118–126
22. Zhang WM, Wu XL, Hu JS, Guo YG, Wan LJ (2008) Carbon coated Fe_3O_4 nanospindles as a superior anode material for lithium-ion batteries. Adv Funct Mater 18:3941–3946
23. Lou XW, Wang Y, Yuan CL, Lee JY, Archer LA (2006) Template-free synthesis of SnO_2 hollow nanostructures with high lithium storage capacity. Adv Mater 18:2325–2329
24. Jiao F, Bruce PG (2007) Mesoporous crystalline β-MnO2-α reversible positive electrode for rechargeable lithium batteries. Adv Mater 19:657–660
25. Grugeon S, Laruelle S, Urbina RH, Dupont L, Poizot P, Tarascon JM (2001) Particle size effects on the electrochemical performance of copper oxides toward lithium. J Electrochem Soc 148: A285–A292
26. Maier J (2005) Nanoionics: ion transport and electrochemical storage in confined systems. Nat Mater 4:805–815
27. Cao AM, Hu J, Liang HP, Wan LJ (2005) Self-assembled vanadium pentoxide (V_2O_5) hollow microspheres from nanorods and their application in lithium-ion batteries. angew. chem. Int Ed 44:4391–4395
28. Zhang Y, Bakenov Z, Zhao Y, Konarov A, Doan TNL, Malik M, Paron T, Chen P (2012) One-step synthesis of branched sulfur/polypyrrole nanocomposite cathode for lithium rechargeable batteries. J. Power Sources 208:1–8
29. Zhang Y, Zhao Y, Yermukhambetova A, Bakenov Z, Chen P (2013) Ternary sulfur/polyacrylonitrile/$Mg_{0.6}Ni_{0.4}O$ composite cathodes for high performance lithium/sulfur batteries. J Mater Chem A 1: 295–301